Research Paper

Persistent free radicals in biochar enhance superoxide-mediated Fe(III)/Fe (II) cycling and the efficacy of CaO_2 Fenton-like treatment

Shuqi Zhang [a], Yan Wei [a], Jordin Metz [b], Shengbing He [a], Pedro J.J. Alvarez [b], Mingce Long [a,*]

[a] School of Environmental Science and Engineering, Key Laboratory of Thin Film and Microfabrication Technology (Ministry of Education), Shanghai Jiao Tong University, 800 Dongchuan Road, Shanghai 200240, China
[b] Rice University, Houston, TX 77005, United States
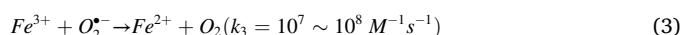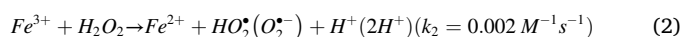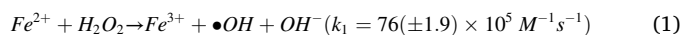
ARTICLE INFO

ABSTRACT

Superoxide radicals ($O_2^{\bullet-}$) produced by the reaction of Fe(III) with H_2O_2 can regenerate Fe(II) in Fenton-like reactions, and conditions that facilitate this function enhance Fenton treatment. Here, we developed an efficient Fenton-like system by using calcium peroxide/biochar (CaO_2/BC) composites as oxidants and tartaric acid-chelated Fe(III) as catalysts, and tested it for enhanced $O_2^{\bullet-}$-based Fe(II) regeneration and faster sulfamethoxazole (SMX) degradation. SMX degradation rates and peroxide utilization efficiencies were significantly higher with CaO_2/BC than those with CaO_2 or H_2O_2 lacking BC. The CaO_2/BC system showed superior activity to reduce Fe(III), while kinetic analyses using chloroform as a $O_2^{\bullet-}$ probe inferred that the $O_2^{\bullet-}$ generation rate by CaO_2/BC was one-half of that by CaO_2. Apparently, $O_2^{\bullet-}$ is utilized more efficiently in this system to regenerate Fe(II) and enhance SMX degradation. Additionally, a positive correlation between SMX degradation rate constants and EPR signal intensities of biochar-derived persistent free radicals (PFRs) in CaO_2/BC was obtained. We postulate that PFRs enhanced Fe(III) reduction by shuttling electrons donated by $O_2^{\bullet-}$. This represents a new strategy to augment the ability of superoxide to accelerate Fe(III)/Fe(II) cycling for increased hydroxyl radical production and organic pollutant removal in Fenton-like reactions.

1. Introduction

Fenton and Fenton-like systems are widely used to remove refractory organic contaminants in wastewater (Qin et al., 2015; Thomas et al., 2021) or soil (Yang et al., 2019) due to their effectiveness in producing reactive oxygen species (ROS) by using hydrogen peroxide (H_2O_2) and iron-based catalysts (Liu et al., 2021; Wang and Tang, 2021a). Among the various involved ROS, hydroxyl radicals ($\bullet OH$) that are generated from the fast reduction of H_2O_2 by Fe(II) (Eq. 1) (Pham et al., 2009) play a dominant role in organic oxidation (Wang et al., 2021b; Yang et al., 2018, 2021). However, this reaction oxidizes Fe(II) to Fe(III), and the subsequent regeneration of Fe(II) by H_2O_2 is sluggish (Eq. 2) (Hou et al., 2017; Zhou et al., 2020; Zhu et al., 2020a), which greatly limits the efficiency of this advanced oxidation system. The simultaneously generated superoxide ($O_2^{\bullet-}$) is another important ROS (Eq. 2), which facilitates the reduction of Fe(III) (Eq. 3) (Li et al., 2016; Pan et al., 2018). However, due to the low yield and poor reactivity of $O_2^{\bullet-}$ in water, slow Fe(III)/ Fe(II) cycling remains the bottleneck in Fenton based treatment technologies (Pignatello et al., 2006; Rose and Waite,

2005; Xing et al., 2018).

$$Fe^{2+} + H_2O_2 \rightarrow Fe^{3+} + \bullet OH + OH^- (k_1 = 76(\pm 1.9) \times 10^5 \, M^{-1}s^{-1}) \quad (1)$$

$$Fe^{3+} + H_2O_2 \rightarrow Fe^{2+} + HO_2^{\bullet}(O_2^{\bullet-}) + H^+ (2H^+)(k_2 = 0.002 \, M^{-1}s^{-1}) \quad (2)$$

$$Fe^{3+} + O_2^{\bullet-} \rightarrow Fe^{2+} + O_2 (k_3 = 10^7 \sim 10^8 \, M^{-1}s^{-1}) \quad (3)$$

Several strategies have been developed to promote $O_2^{\bullet-}$ production and accelerate Fe(II) regeneration and Fenton-like reactions (Huang et al., 2021). Metal ions, such as Mn^{2+}, can react with Fe (III)-nitrilotriacetic acid complexes and promote $O_2^{\bullet-}$ production in homogeneous systems (Li et al., 2016). Chelates like ethylenediamine-N,N′-disuccinic acid can serve as superoxide radical-promoting agents to enhance $O_2^{\bullet-}$ production (Huang et al., 2013; Rastogi et al., 2009). Metal peroxides (Xue et al., 2019) such as CaO_2 (Tang et al., 2020) and MgO_2 (Yuan et al., 2019; Zhu et al., 2020b) produce $O_2^{\bullet-}$ three orders of magnitude faster than H_2O_2 due to their intrinsic reducibility. However, the increase of $O_2^{\bullet-}$ yield sacrifices the utilization efficiency of oxidants, because the superoxide radicals eventually convert into O_2 by reducing

---

* Corresponding author.
  E-mail address: long_mc@sjtu.edu.cn (M. Long).

Fe(III) (Eq. 3) (Furman et al., 2009; Hayyan et al., 2016). Furthermore, superoxide is essentially unreactive in water due to the formation of hydrogen bonds and rapid disproportionation into O_2 and H_2O_2 (Furman et al., 2009). However, increasing the yield of $O_2^{\bullet-}$ should compensate for its low reactivity in water. Therefore, it is important to explore approaches to enhance the participation of $O_2^{\bullet-}$ to accelerate Fe(III) reduction (for faster Fe(III)/Fe(II) cycling) without decreasing utilization efficiency of peroxides.

Although aprotic solvents can effectively enhance $O_2^{\bullet-}$ reactivity by suppressing the formation of hydrogen bonds, there are very few reports about the enhancement of $O_2^{\bullet-}$ reactivity in water (Javed et al., 2020; Sawyer and Valentine, 1981; Smith et al., 2004). High H_2O_2 concentrations (> 0.3 M) that are frequently used in catalyzed H_2O_2 propagations in soil remediation can increase the production of $O_2^{\bullet-}$ (Mitchell et al., 2014). However, this approach is not feasible for water treatment because H_2O_2 at a high concentration can scavenge hydroxyl radicals and decrease the degradation efficiency of organic pollutants (Pignatello et al., 2006). Solid interfaces were reported to increase the reactivity of $O_2^{\bullet-}$ generated from KO_2, and to facilitate hexachloroethane (HCA) degradation (Furman et al., 2009). However, these reactions are not Fenton-like, and the mechanism responsible for the enhanced reactivity of $O_2^{\bullet-}$ is unclear. Overall, modulating and increasing $O_2^{\bullet-}$ participation in Fenton-like reactions remains a significant technical challenge.

In this study, we used a CaO_2-biochar system to enhance $O_2^{\bullet-}$ utilization for improving Fe(III)/Fe(II) cycling in Fenton-like reactions. Biochar (BC) is a carbonaceous material obtained mainly from biomass pyrolysis (Sun et al., 2021), and has recently found wide applications in soil amendments (Liao et al., 2014), carbon storage (Sanchez et al., 2001), and heavy metal immobilization (Tian et al., 2019; Wang and Wang, 2019a). It is well-known that BC contains abundant persistent free radicals (PFRs) (Chen et al., 2020; Yang et al., 2016). These resonance-stabilized radicals, such as semiquinones and phenoxyls, serve as both electron donors and electron acceptors and participate in redox reactions (Klupfel et al., 2014; Yu et al., 2015; Zhong et al., 2019). However, there are very few reports on the influence of BC on the transformation and reactivity of ROS, which may be a missed opportunity for enhancing Fenton's reactions. In this work, we fabricated CaO_2/BC based Fenton-like systems to enhance Fe(III)/Fe(II) cycling (and associated hydroxyl radical production) via superoxide-PFR interactions, and demonstrated the benefits of this novel approach for efficient sulfamethoxazole (SMX) degradation.

2. Materials and methods

2.1. Materials

All chemicals used and their sources are described in Supporting Information (Text S1). BC_T was synthesized by calcining rice husk at different temperatures (T = 300, 400, 500 and 600 °C) according to previous procedures (Qin et al., 2016). Without specification, the BC in the oxidants was calcined at 400 °C.

2.2. CaO_2/BC preparation

CaO_2/BC with different mass ratios of CaO_2 to BC was synthesized by using $Ca(OH)_2$ and H_2O_2 as precursors (Li et al., 2020). Briefly, a given weight of BC was dispersed in 7 mL deionized water by magnetically stirring at 40 °C. Next, 2.5 g $Ca(OH)_2$ and 4.35 mL of H_2O_2 (30 wt%) were successively added into the suspension. After magnetically stirring the mixture for 1 h, the powder was obtained by filtering, washing with ethanol, and drying at 30 °C for 12 h. The obtained materials were named as CaO_2/BC-x (x = 1, 2, 4 and 6), where x represents the mass ratio of CaO_2 to BC. If not specified (without the label x), the mass ratio was 2 for CaO_2/BC.

2.3. SMX degradation in Fenton-like reactions

The performance of the Fenton-like reactions was assessed by the removal of the recalcitrant sulfonamide antibiotic, sulfamethoxazole (SMX). In a typical test, 1.2 mM tartaric acid (TA) and 0.6 mM $Fe(NO_3)_3$ were added into 10 mg/L SMX solution (initial pH 7.0) in a 100 mL reactor under magnetic stirring (450 rpm) at 20 °C. The pH decreased to 2.6 after mixing for 20 min due to the addition of TA and the hydrolysis of Fe (III). CaO_2/BC (1.2 mM peroxide dosage) was then added to initiate the reactions, and the final pH increased to 6.7 after 20 min due to the formation of $Ca(OH)_2$.

A conventional Fenton reaction was also carried out (for benchmarking) using the same procedure, except that 0.6 mM $Fe_2(SO_4)_3$ and 1.2 mM H_2O_2 were used without addition of TA, and the pH was adjusted to 2.6 with H_2SO_4 (1 M). Samples were withdrawn at a given interval, filtered and quenched by equal volumes of methanol. To evaluate the contribution of radicals, scavenging tests were carried out by using tertiary butanol (TBA) and chloroform as the scavengers of •OH and $O_2^{\bullet-}$, respectively. All experiments were performed in triplicate, and the results were reported as the mean values with standard deviations. Student's t-test was conducted to evaluate the significance of the differences between treatments at the 95% confidence level (p < 0.05).

2.4. Analytical methods

The crystal phases of CaO_2 and CaO_2/BC were examined on a Rigaku D/max-2200/PC X-Ray diffractometer (XRD). The surface functional groups were analyzed by a Fourier transform infrared spectrometer (FTIR, Nicolet 6700, Thermo, USA). The Raman spectra were measured on an inVia Qontor Raman spectrometer (Renishaw, Britain) with 532-nm excitation from a 25-mW He-Ne Laser. The morphologies of the samples were collected and observed on a field emission scanning electron microscope (FE-SEM, Nova NanoSEM 450, FEI). XPS analyses were performed on an Axis Ultra DLD system (Shimadzu/Kratos) of X-ray photoelectron spectroscopy (XPS).

H_2O_2 concentrations were determined by a modified metavanadate method (Wei et al., 2021). The amount of peroxides in CaO_2/BC-x and CaO_2 was measured by a potassium permanganate ($KMnO_4$) titration method (Wu et al., 2019; Zhu et al., 2020b). The purity of these peroxide composites (which decreases with the presence of $Ca(OH)_2$) was determined based on the ratio of the measured peroxide content to the theoretical stoichiometric content.

The reactive oxygen species (•OH, $O_2^{\bullet-}$ and $^1O_2$) were detected by electron paramagnetic resonance (EPR) spectrometry (ELEXSYS E580, Bruker). The sweep field ranged from 3400 G to 3500 G, and microwave power and frequency were set at 15 mW and 9.67 GHz. 5,5-dimethyl-1-pyrroline-N-oxide (DMPO) and 2,2,6,6-tetramethylpiperidine (TEMP) were used as the spin traps. The amount of dissolved ferrous ions was analyzed by a modified 1,10-phenanthroline chromogenic method. Quantitative analyses of residual SMX concentrations were performed on a high-performance liquid chromatography (HPLC, LC-20 CE, Shimadzu) equipped with a Shim Pack C18 chromatographic column (ZORBAX Eclipse XDBC18) and a UV–vis detector (SPD-20AV). The concentration of hexachloroethane (HCA) was determined on a Gas Chromatograph-Triple Quadrupole Tandem Mass Spectrometer (GCMS-QP2020, Shimadzu). The amount of total organic carbon (TOC) in the SMX degradation was determined by a TOC/TN analyzer (multi N/C 3100, Analytik Jena).

3. Results and discussion

3.1. CaO_2/BC Fenton-like system efficiently utilizes peroxides to accelerate SMX degradation

SMX degradation was used to evaluate the performance of Fenton-like systems with various oxidants. Fig. 1(a) shows that BC or $Ca(OH)_2$
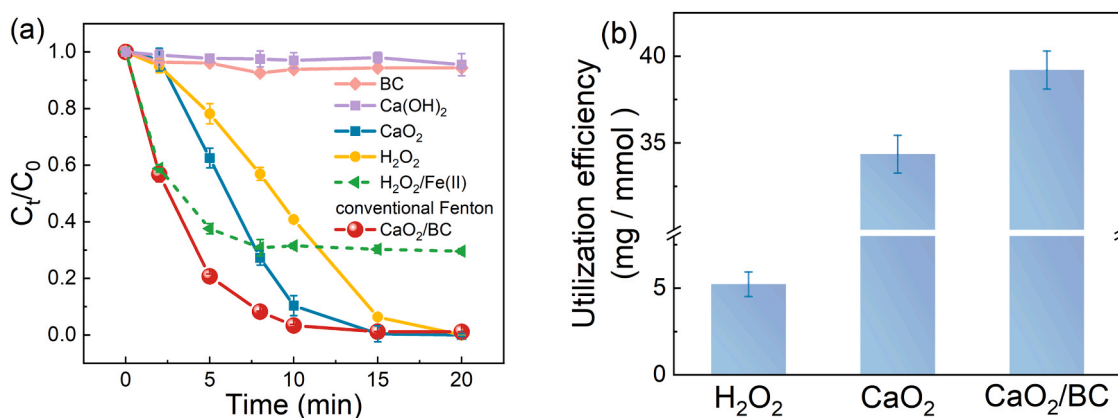
Fig. 1. (a) SMX degradation and (b) peroxide utilization efficiency in different reaction systems. All reactions contained $[SMX]_0 = 10$ mg/L, $[Fe(III)] = 0.6$ mM, n_{Fe}: $n_{TA} = 1:2$, $[BC] = 64$ mg/L and [peroxides] = 1.2 mM. The initial pH of the SMX solution was 7.0; this decreased to pH 2.6 after the addition of Fe(III)-TA, and increased to final pH 6.7; no TA was added in the conventional Fenton system.

(the hydrolysis product of CaO_2) alone removed less than 5% SMX in 20 min, indicating that SMX adsorption on BC or $Ca(OH)_2$ was minor. The systems with oxidants (H_2O_2 and/or CaO_2) showed faster SMX removal (Fig. 1a). TA was used as the complexing agent to stabilize iron over a wide pH range and prevent its precipitation when the pH increased to 6.7 during the reaction (due to $Ca(OH)_2$ production). SMX degradation in these systems was fitted by a pseudo-first-order kinetic model. The observed reaction rate constant (k_{obs}) of the H_2O_2-based system was 0.17 ($\pm$ 0.007) min^{-1}. This value was 0.22 ($\pm$ 0.003) min^{-1} in the CaO_2 system, and SMX removal efficiency reached 99% at 15 min. The better performance of CaO_2-based Fenton-like reactions is ascribed to the enhanced yield of superoxide radicals, which promotes the recycling of Fe(III) to Fe(II) (Pan et al., 2018; Wang et al., 2016). In contrast, the conventional Fenton system (Fe(II)/H_2O_2) resulted in fast initial SMX degradation rate (0.19 $\pm$ 0.013 min^{-1}, first 5 min) due to the prompt H_2O_2 decomposition and •OH production, but the SMX degradation rate was very slow after 8 min and about 37% of SMX (10 mg/L initially) remained in the system (Fig. 1a). This can be attributed to Fe(III) accumulation and sluggish Fe(II) regeneration.

The synthesized CaO_2/BC system has the highest SMX degradation rate coefficient (0.34 $\pm$ 0.014 min^{-1}), which was 1.5 times that of the CaO_2 system without BC and 1.7 times higher than the traditional Fenton system. By using the CaO_2/BC composite as the oxidant, SMX removal efficiency reached 96% at 10 min. As a control, a mixture made by adding BC powder into the CaO_2 system to create a hybrid system (h-CaO_2/BC) was tested; this slightly increased the k_{obs} to 0.24 ($\pm$ 0.013) min^{-1}, about 9% more than the CaO_2 system without BC (Fig. S1a). The results indicate that the close contact between BC and CaO_2 favors electron transfer and promotes the Fenton-like oxidation of SMX. Furthermore, in the absence of iron, the direct interaction between BC and H_2O_2 did not induce significant SMX degradation in 20 min (Fig. S1b), indicating that the contribution of H_2O_2 activation by BC was negligible for SMX degradation. These experiments show that the presence of BC effectively accelerated SMX degradation in the CaO_2/BC Fenton-like reactions, significantly outperforming the controls and the traditional Fenton treatment (Fig. 1a). Adding BC powder to the H_2O_2/ Fe(III) system slightly increased k_{obs} from 0.17 ($\pm$ 0.007) to 0.19 ($\pm$ 0.0053) min^{-1} (Fig. S2), suggesting its potential to also enhance conventional Fenton treatment.

The utilization efficiency of peroxides, that is, the total removed TOC per consumed peroxides, in various Fenton-like systems was estimated by measuring the residual H_2O_2 and TOC. The utilization efficiency (at the 20th min) for the H_2O_2 system (in terms of dissolved TOC removal) was only 5 mg-TOC per mmol peroxides (Fig. 1b and Fig. S3). The poor performance may be attributed to disproportionation of H_2O_2 and low mineralization of organics. In contrast, the utilization efficiencies of the

CaO_2 and CaO_2/BC systems were significantly improved, reaching 34 and 39 mg TOC removed/mmol peroxides, respectively. The peroxide utilization efficiency was also evaluated based on SMX removal, and was significantly higher for the CaO_2/BC system than for the systems with H_2O_2 or CaO_2 alone (i.e., 52.6 vs. 12.1 and 12.6 mg-SMX/mmol peroxides, respectively, Fig. S4). These results imply that the peroxides utilization efficiency is much higher for CaO_2 than for H_2O_2, and the incorporation of BC can simultaneously accelerate SMX degradation and improve the peroxide utilization efficiency.

The effect of mass ratios of CaO_2 to BC on SMX degradation was investigated while holding constant the peroxide concentration in each reaction (Fig. 2a). SMX removal was accelerated with increasing BC content, up to 100% removal in 15 min. However, the CaO_2/BC-2 and CaO_2/BC-4 systems showed similar kinetics of SMX degradation, achieving 97% SMX removal in 8 min. Further increasing the BC content to 50% (composite CaO_2/BC-1) resulted in a decreased SMX removal efficiency, since too much BC apparently inhibits ROS generation. The purity (in terms of peroxide content) of the composite oxidants increased with increasing BC content (Fig. 2b), which may be due to BC facilitating uniform dispersion of $Ca(OH)_2$ and its transformation to CaO_2. The first-rate constants (k) were shown in Fig. 2(b), in which CaO_2/BC-2 exhibited the highest k value (0.34 $\pm$ 0.014 min^{-1}). Thus, CaO_2/BC-2 was selected for further tests.

The compositions and structures of the optimized CaO_2/BC were explored. Raman spectroscopy showed a strong peak for CaO_2/BC at 845 cm^{-1} (Fig. 2c), corresponding to the expected O–O stretching vibration in CaO_2 (Wu et al., 2018). However, the peak slightly positively shifted compared to that of CaO_2 (843 cm^{-1}), which can be attributed to that the chemical environment of peroxide bonds changed after the incorporation of BC (Guo et al., 2015). In the FTIR spectra, the absorption bands at 875 cm^{-1} were attributed to the O–O bridge of CaO_2 (Fig. S5a) (Żeglinski et al., 2006), and the two peaks at 1410 and 1490 cm^{-1} were ascribed to O–Ca–O bending vibrations (Yan et al., 2009). The band corresponding to the stretching vibration of C–O–C in BC, located at 1051 cm^{-1}, shifted to 1076 cm^{-1} in the spectrum of CaO_2/BC; this indicates a strong interaction between CaO_2 and BC, which facilitates interactions between the released ROS and proximal BC (Li et al., 2020). The XRD patterns suggest that tetragonal-phase CaO_2 (JCPDS Card 85-514) is formed in the CaO_2/BC composites (Fig. S5b) (Wang et al., 2019b). The morphology of BC and CaO_2/BC was characterized by SEM (Fig. S5c and d). BC had a porous structure, while CaO_2/BC exhibited spherical CaO_2 particles dispersed on the surface of BC. There was agglomeration of CaO_2 particles due to their high surface energy (Wu et al., 2019). The strong peak at g = 2.0021 in the EPR spectra of BC proved the existence of PFRs. The peak shifted to g = 2.0037 for CaO_2/BC (Fig. 2d), which may be attributed to the
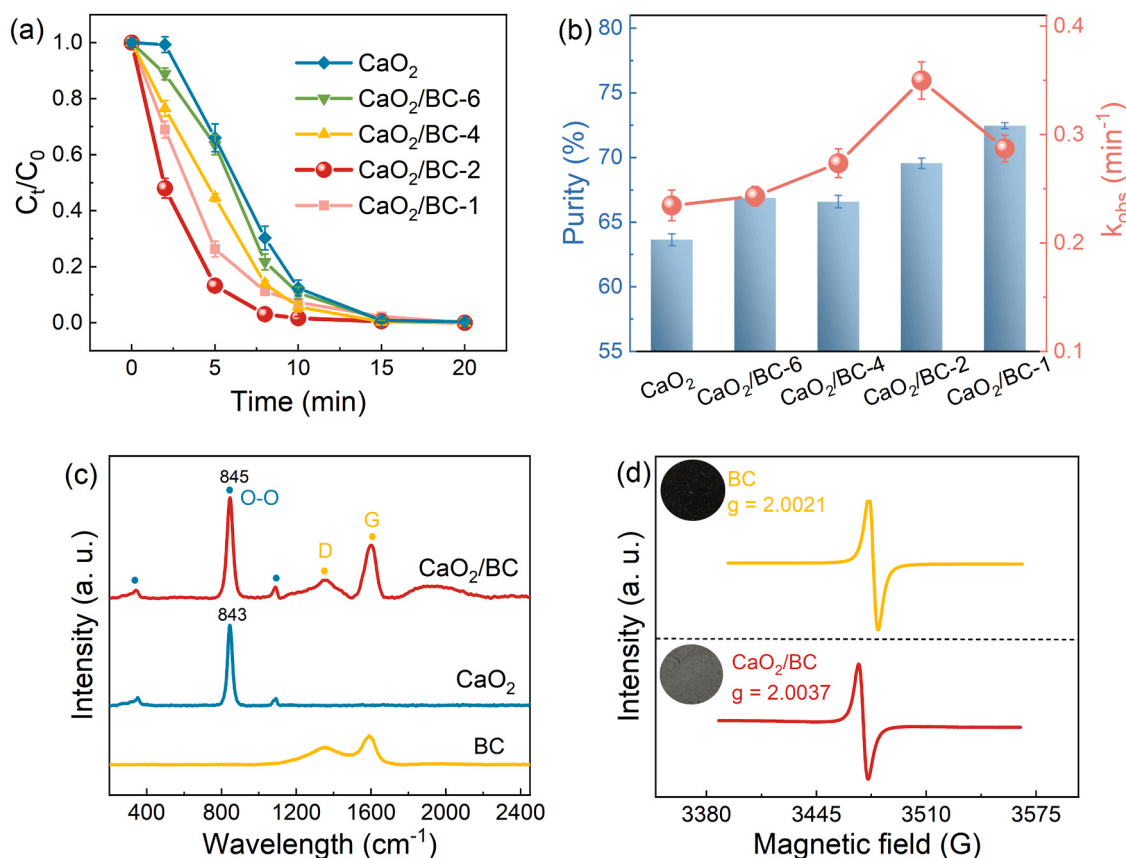
**Fig. 2.** The effect of mass ratios of CaO$_2$ to BC on (a) SMX degradation (CaO$_2$/BC-*x*, where *x* is the mass ratio of CaO$_2$ to BC, and as *x* decreases so does the proportion of CaO$_2$) and (b) peroxide purity and SMX degradation rate constants; (c) Raman spectra of CaO$_2$/BC, CaO$_2$ and BC; (d) EPR spectra of CaO$_2$/BC and BC ([SMX]$_0$ = 10 mg/L, [Fe(III)] = 0.6 mM, n_{Fe}:n_{TA} = 1:2, [BC] = 64 mg/L, [peroxides] = 1.2 mM).

transformation of PFRs from carbon centered types into carbon-oxygen centered types due to the incorporation of peroxides (Xin et al., 2021; Zhong et al., 2018). These data show that a CaO$_2$ and BC composite with a significant amount of PFRs was obtained.

The effects of the molecular ratio of Fe(III) to TA (R$_{Fe/TA}$), total iron concentrations, oxidant dosages, and initial pH on SMX degradation in the CaO$_2$/BC systems were investigated (Fig. S6). The optimal R$_{Fe/TA}$ and iron concentration were 1:2 and 0.6 mM, respectively. Significant SMX degradation was achieved at a wide initial pH range (from 3.0 to 10.0). This could be attributed to TA serving as the chelator to stabilize Fe(III). Excess TA exerts steric hindrance on Fe^{2+}, hindering the reaction

between the complex and H$_2$O$_2$ generated by CaO$_2$/BC (Tang et al., 2020). SMX removal efficiency increased with increasing CaO$_2$/BC dosage from 0.4 to 1.2 mM, but was strongly inhibited with further increases in oxidant content since excess CaO$_2$/BC increased the slurry's pH (to about pH 11.3 at 2.0 mM peroxides) (Tang et al., 2020; Yan et al., 2021). Significant SMX degradation was achieved at a wide initial pH range (from 3.0 to 10.0), which could be attributed to TA chelating and stabilizing Fe(III). Overall, the CaO$_2$/BC system shows satisfactory activity at a wide range of pH values, enhancing its utility for application in a wide range of environments.
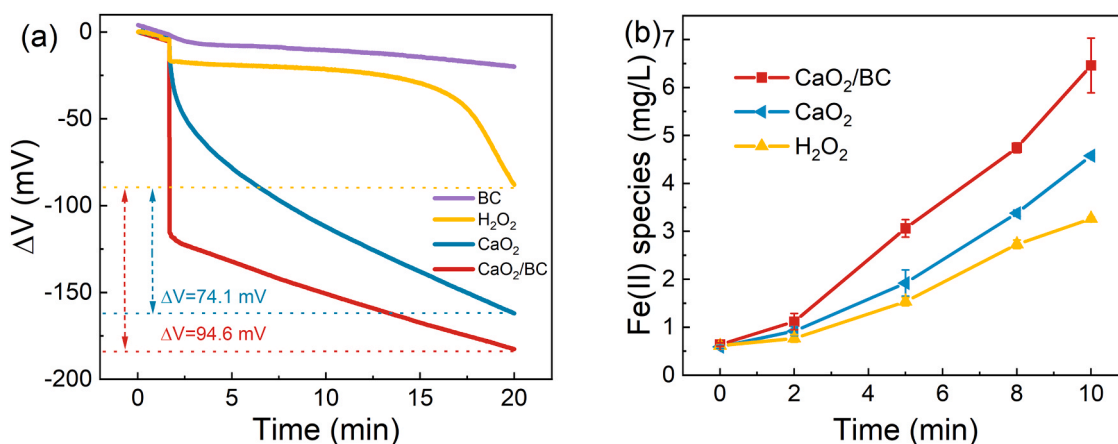
Fig. 3. (a) Changes of open circuit potentials of Pt electrodes and (b) dissolved Fe(II) in different Fenton-like systems ([SMX]$_0$ = 10 mg/L, [Fe(III)] = 0.6 mM, n_{Fe}: n_{TA} = 1:2, [BC] = 64 mg/L, [peroxides] = 1.2 mM).

3.2. The CaO$_2$/BC system enhanced Fe(II) regeneration

In Fenton-like systems, reductants such as superoxide are important to regenerate Fe(II) and subsequently produce hydroxyl radicals. Reduction activity in each Fenton-like system was evaluated by measuring the changes of open-circuit potentials (ΔV) at the Pt electrode. The ΔV value was relatively constant in the BC alone system and declined immediately with the addition of all oxidants (Fig. 3a), suggesting the decrease of redox potentials in the systems. This can be attributed to the generation of reducing constituents such as Fe(II) and superoxide radicals (Barreiro et al., 2007; Chen et al., 2002; Pan et al., 2018). The trend of the Fenton-like systems with a greater ΔV was consistent with that of SMX degradation efficiencies in the corresponding systems. The decreased open-circuit potentials at the 20th min in CaO$_2$ and CaO$_2$/BC systems are 74.1 mV and 94.6 mV more than that of the H$_2$O$_2$ system, respectively. This suggests that more reductive substances are generated in both CaO$_2$ containing systems, and that BC promotes the generation of reductive substances in the reactions. The ΔV values in the absence of the chelating agent (TA) were also measured (Fig. S7). The order of ΔV in the absence of TA is the same as that in the presence of TA, revealing that BC was critical for the increased reduction potentials and promoted SMX oxidation.

The concentration of Fe(II) in each system was compared to show the enhanced generation of reductive substances in the Fenton-like reactions (Fig. 3b). Fe(II) concentrations increased as the reaction progressed; the CaO$_2$/BC system had the highest concentration of Fe(II), followed by the CaO$_2$ and H$_2$O$_2$ systems. The results are consistent with the open-circuit potential measurements. It is known that BC has the potential to directly reduce Fe(III) due to its ability to serve as an electron donor that has a capacity in the range of 0.24–1.83 mmol electrons/g (Chacón et al., 2020; Xu et al., 2020; Zhang et al., 2018). However, the actual contribution of BC alone to the generation of Fe(II) is negligible, and the reduction kinetics by BC-only control systems are sluggish (Fig. S8). The final concentrations of Fe(II) at 10 min in the presence of BC or BC and TA were only 0.09 mg/L and 0.61 mg/L, much lower than that observed in the CaO$_2$/BC Fenton-like system (6.45 mg/L), which may be due to the low reduction potential of electrons in BC. Thus, Fe(II) generation was promoted by the presence of BC in the CaO$_2$/BC system, which subsequently favors hydroxyl radical production and SMX degradation (Fig. 1a).

3.3. Higher superoxide reactivity in the CaO$_2$/BC system was a critical enhancing factor

Although •OH is the main ROS responsible for treatment in Fenton-like systems, O$_2$$^{•−}$ played a significant indirect role in enhancing •OH production and SMX treatment, as detailed below. The main ROS contributing to SMX degradation in the CaO$_2$ and CaO$_2$/BC systems were evaluated by EPR analysis and scavenging tests. In the EPR spectra, the characteristic four peaks with an intensity ratio of 1:2:2:1 for the hydroxyl-radical adduct DMPO-OH were observed in both the CaO$_2$ and CaO$_2$/BC systems (Fig. 4a inset and Fig. S9) (Han et al., 2014; Qin et al., 2021). Fig. 4(a) compares the signal intensities of DMPO-OH adducts in the two systems at different times, and corroborates that the CaO$_2$/BC system produced significantly higher concentrations of •OH (p < 0.05) to facilitate SMX degradation. Furthermore, tertbutyl alcohol (TBA) was used to scavenge hydroxyl radicals ($k_{•OH/TBA} = 6.0 \times 10^8 \ M^{-1}s^{-1}$) (Buxton et al., 1988). SMX degradation was almost completely inhibited in the presence of TBA, corroborating the critical role of •OH in both treatment systems (Fig. 4b).

The characteristic six peaks for the superoxide-radical adduct DMPO-OOH were observed in both the CaO$_2$ and CaO$_2$/BC systems (Fig. S10). With the addition of 10 mM chloroform as the scavenger of superoxide radicals ($k_{O_2^{•−}/chloroform} = 3.0 \times 10^{10} \ M^{-1}s^{-1}$) (Buxton et al., 1988), the SMX degradation rate constant for the CaO$_2$ system (Fig. 4b) decreased by 80% (from 0.22 ± 0.003–$0.048 \pm 0.003 \ min^{-1}$), while that for CaO$_2$/BC decreased more significantly by 96% (from 0.34 ± 0.014–$0.014 \pm 0.001 \ min^{-1}$). This indicates that superoxide radicals contribute to the CaO$_2$/BC system's higher treatment efficiency.

While scavenger tests indicate that hydroxyl radical is the most important radical contributing to SMX degradation (Fig. 4b and Fig. S11), superoxide clearly plays a significant role as a reductant in the enhanced degradation mechanism of the CaO$_2$/BC system. The importance of O$_2$$^{•−}$ in this treatment system was demonstrated by using various concentrations of chloroform, which serves as a probe that reacts with O$_2$$^{•−}$ (Huang et al., 2013; Pan et al., 2018). As shown in Fig. 5(a) and Fig. S12a, SMX removal efficiencies for both CaO$_2$ and CaO$_2$/BC systems were progressively inhibited as chloroform concentrations (and thus superoxide scavenging) increased. Note that the relationship between the initial SMX degradation rates ($R_{SMX}^d \ M \bullet s^{-1}$) and chloroform dosages was well fitted by a hyperbolic function (Eq. 4).

$$R_{SMX}^d = \frac{R_{O_2^{•-}}^f \times k_{SMX,O_2^{•-}} \times c_{SMX}}{k_{chloroform,O_2^{•-}} \times c_{chloroform} + k_{SMX,O_2^{•-}} \times c_{SMX} + k_{Fe^{III}-TA,O_2^{•-}} \times c_{Fe^{III}-TA}} \tag{4}$$

where, $R_{O_2^{•-}}^f$ is the formation rate of O$_2$$^{•−}$ ($M \ s^{-1}$), and $k_{SMX,O_2^{•-}}$, $k_{chloroform,O_2^{•-}}$, and $k_{Fe^{III}-TA,O_2^{•-}}$ are second-order rate constants of superoxide radicals reacting with SMX, chloroform, or $Fe^{III} - TA$,
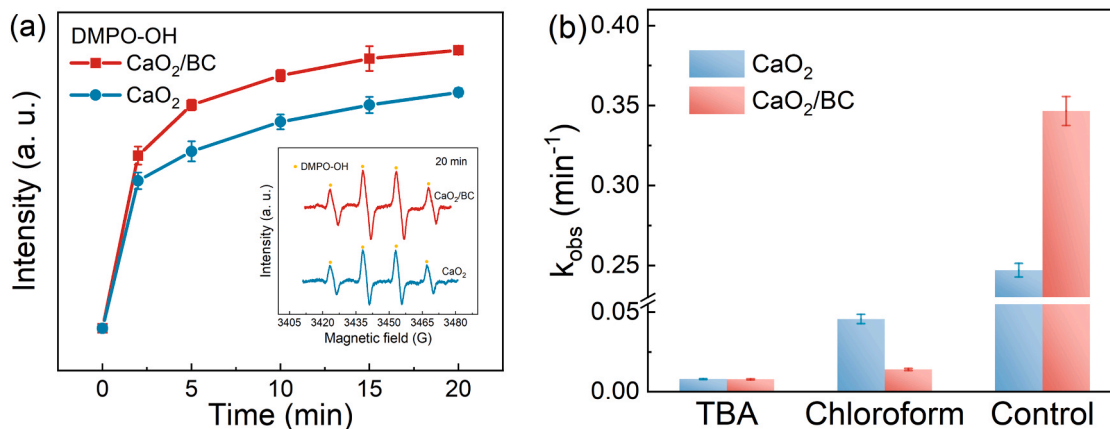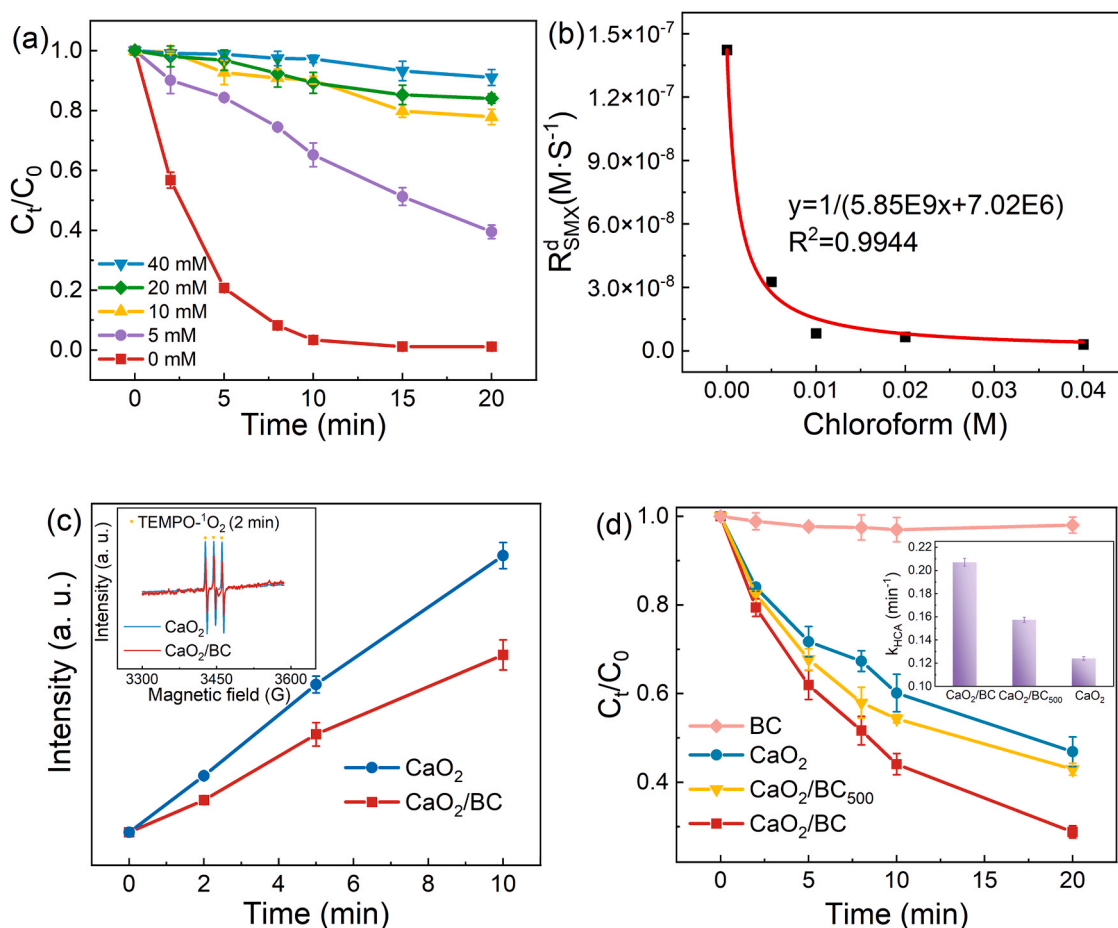

Fig. 4. (a) EPR signal intensity over time of DMPO-OH (hydroxyl radical adduct) in CaO$_2$/BC and CaO$_2$ system (inset shows EPR signals of DMPO-OH at 20 min); (b) Effect of scavengers on SMX degradation in various systems ([SMX]$_0$ = 10 mg/L, [Fe(III)] = 0.6 mM, n$_{Fe}$: n$_{TA}$ = 1:2, [peroxides] = 1.2 mM, [TBA] = 10 mM, [chloroform] = 10 mM).

Fig. 5. (a) Effect of chloroform concentration on SMX degradation in CaO$_2$/BC system; (b) initial degradation rate of SMX (R^d_{SMX}) as a function of chloroform concentrations in CaO$_2$/BC system; (c) the evolution of signal intensities of TEMPO-^{1}O$_2$ adducts in the presence of 10 mM TBA and (d) HCA degradation in the CaO$_2$ and CaO$_2$/BC systems ([SMX]$_0$ = 10 mg/L, [HCA]$_0$ = 500 μg/L, [Fe(III)] = 0.6 mM, n_{Fe}:n_{TA} = 1:2, [peroxides] = 1.2 mM, pH$_0$ = 7.0). Inset in (c) is the TEMP-^{1}O$_2$ signals at 2 min, and that in (d) is the HCA degradation rate constants in different systems.

respectively. The $R^f_{O_2^{\bullet-}}$ in the CaO$_2$ and CaO$_2$/BC systems can be calculated by Eq. (5) based on the fitting parameter a (Huang et al., 2013; Pan et al., 2018).

$$R^f_{O_2^{\bullet-}} = \frac{k_{chloroform,O_2^{\bullet-}}}{a \times k_{SMX,O_2^{\bullet-}} \times c_{SMX}} \tag{5}$$

Although the value of $k_{SMX,O_2^{\bullet-}}$ is unknown, the ratio of the two $R^f_{O_2^{\bullet-}}$ values for the CaO$_2$/BC (Fig. 5b) and CaO$_2$ (Fig. S12b) systems can be obtained from the inverse ratio of parameter a (Text S3). Surprisingly, $R^f_{O_2^{\bullet-}}$ in the CaO$_2$ system was 2.1 times that of the CaO$_2$/BC system. Control tests indicated that the difference in H$_2$O$_2$ release from CaO$_2$ versus CaO$_2$/BC systems was negligible during the first 30 min (Fig. S13). These results unequivocally demonstrate that the presence of BC decreases the yield of O$_2^{\bullet-}$ from CaO$_2$. This may be explained by the fact that the CaO$_2$/BC system produces more ferrous species (Fig. 3b), which promote the conversion of peroxides into hydroxyl radicals (Eq. 1) and simultaneously decrease reaction rates between peroxides and ferric ions (Eq. 2) that produce superoxide. The decreased O$_2^{\bullet-}$ yield by incorporating BC is also consistent with the results on the enhanced utilization efficiency of peroxides in CaO$_2$, because less O$_2^{\bullet-}$ production can avoid the consumption of peroxides through a reductive pathway. Taken together, these results indicate that O$_2^{\bullet-}$ produced by the CaO$_2$/BC system is more efficiently used to reduce Fe(III) to Fe(II) (and thus enhance •OH production) compared to the CaO$_2$ control.

Lower O$_2^{\bullet-}$ production in the CaO$_2$/BC system compared to controls

was corroborated by the detection of ^{1}O$_2$ using EPR spectroscopy. In Fenton-like reactions, ^{1}O$_2$ can be produced by O$_2^{\bullet-}$ disproportionation (Eq. 6, $k = 2.4 \times 10^{12-pH} M^{-1}s^{-1}$) (Wang et al., 2020). Since •OH can increase the generation of ^{1}O$_2$ by participating a series of radical reactions (Yi et al., 2019; Dou et al., 2019), the experiments were conducted in the presence of TBA, a hydroxyl radical scavenger. Under these conditions of suppressed •OH generation, the produced ^{1}O$_2$ is positively correlated with the amount of O$_2^{\bullet-}$ produced (Nosaka and Nosaka, 2017; Ali et al., 2020).

$$2O_2^{\bullet-} + 2H_2O \rightarrow {}^1O_2 + H_2O_2 + 2HO^- \tag{6}$$

The EPR signal intensities of TEMPO-^{1}O$_2$ in the CaO$_2$ and CaO$_2$/BC systems were detected. The three typical peaks with an intensity ratio of 1:1:1 in both EPR spectra correspond to the spin adduct of TEMPO-^{1}O$_2$ (Duan et al., 2018; Miao et al., 2020). The intensity of TEMPO-^{1}O$_2$ in the CaO$_2$ system is obviously higher than that of the CaO$_2$/BC system at 2 min (inset in Fig. 5c), demonstrating a higher concentration of ^{1}O$_2$ in the CaO$_2$ system without BC. The evolution of ^{1}O$_2$ concentration in the first 10 min was also monitored (Fig. 5c). When using CaO$_2$/BC as the oxidant, the generation of ^{1}O$_2$ remained lower than that of the CaO$_2$ system within 10 min, which confirms that the presence of BC decreased the production of O$_2^{\bullet-}$. Interestingly, even though the CaO$_2$/BC system produced less O$_2^{\bullet-}$, it recycled Fe(II) faster (Fig. 3b), produced more •OH (Fig. 4a), and (consistently) degraded SMX faster (Fig. 1a). This indicates that O$_2^{\bullet-}$ reactivity is enhanced by BC in the CaO$_2$/BC Fenton-like reactions, contributing to increased SMX removal.

Enhanced O$_2^{\bullet-}$ reactivity with CaO$_2$/BC can be further shown by

hexachloroethane (HCA) degradation tests, because HCA is susceptible to reduction by $O_2^{\bullet-}$ but not to oxidation by $\bullet OH$ (Furman et al., 2009). Only about 2% HCA was removed in the BC alone system (Fig. 5d), indicating that HCA adsorption on BC was minor. The CaO_2/BC based system exhibits a much higher HCA removal efficiency, reaching 71.2% in 20 min. The rate constant of the CaO_2/BC system ($k_{HCA} = 0.2 \pm 0.003$ min^{-1}) was approximately two times higher than that of the CaO_2 system ($k_{HCA} = 0.12 \pm 0.015$ min^{-1}), even though superoxide production in the CaO_2/BC system was lower. These results confirm that the CaO_2/BC system enhances the reactivity of $O_2^{\bullet-}$.

3.4. PFRs in BC promote electron transfer from superoxide to Fe(III)

To explore the critical constituents of BC that enhance $O_2^{\bullet-}$ reactivity, BC with different contents of PFRs were synthesized by calcining rice husk at various temperatures. A series of CaO_2/BC_T ("T" = calcination temperature in ℃) were obtained by using the BC_T as the precursors. PFR content in the CaO_2/BC_T samples can be represented by the EPR intensities. The EPR spectra of the composite oxidants showed that the PFR content is variable (Fig. S14a), and that BC calcined at 400 ℃ had the highest signal intensity and PFR content, which is consistent with previous reports (Fang et al., 2015). The oxidants were used in SMX degradation tests at the same peroxide dosages (Fig. S14b), and apparent reaction rate constants were obtained. A positive linear correlation between SMX degradation rate constants and PFR content was observed (Fig. 6a). SMX degradation was faster with higher PFR content, which facilitated electron transfer from $O_2^{\bullet-}$ to Fe(III) in Fe-TA complexes, and accordingly promoted Fenton-like reactions. The significant contribution of PFRs to $O_2^{\bullet-}$ participation is corroborated by lower HCA degradation activity in the CaO_2/BC_{500} system (Fig. 5d), in which the intensity of PFRs was about one-half of those in CaO_2/BC, indicating lower $O_2^{\bullet-}$ availability in a system with lower PFR content.

PFRs in BC_{400} were reduced by pre-treating BC with 30 wt% H_2O_2 for 40 h to partially eliminate the surface PFRs (Liu et al., 2020; Zhao et al., 2018). A composite labeled as CaO_2/BC_d was synthesized from the treated BC with depleted PFRs. According to the EPR spectra (inset in Fig. 6b), the signal intensity of PFRs in the CaO_2/BC_d was reduced after H_2O_2 treatment. Simultaneously, the SMX degradation performance of CaO_2/BC_d was much poorer than that of the untreated CaO_2/BC, and the k_{obs} values decreased from 0.34 ($\pm$ 0.014) to 0.22 ($\pm$ 0.024) min^{-1}. The EPR signal intensity of PFRs decreased in the CaO_2/BC system after the reaction, while changes in the BC-alone system were negligible (Fig. S15). This indicates the involvement (and consumption) of PFRs in the CaO_2/BC treatment systems, where PFR content in BC would influence $O_2^{\bullet-}$ reactivity towards Fe(II) regeneration (see graphical abstract).

Surface-associated chemical species on fresh and used CaO_2/BC samples were investigated by XPS analyses. The C 1s spectra (Fig. S16) were fitted into three peaks at 284.98 eV, 286.10 eV and 289.02 eV, corresponding to C–C, C–O and C=O, respectively (Ali et al., 2021). The binding energy of C=O decreased from 289.02 to 288.73 eV after reaction, and its percentage increased from 18% to 24%. This suggests that the PFRs were involved in SMX degradation by facilitating electron transfer from carbon related groups on the surface of BC to Fe(III) (Yang et al., 2018). Based on the Fe 2p spectra (Fig. S17), Fe(II) and Fe(III) contents were 54% and 46%, respectively, in the residual CaO_2/BC sample, reflecting the recycling of Fe(III) to Fe(II) on the surface of BC (Zhou et al., 2020). Thus, the XPS results corroborate that PFRs on the surface of BC facilitate Fe(II) regeneration to enhance the efficacy of CaO_2 Fenton-like treatment (see graphical abstract).

Overall, superoxide generated from CaO_2 can interact with PFRs, which are known to serve as electron shuttles and can reduce Fe(III) to regenerate critical Fe(II). Among the diverse types of PFRs in BC, the prevalent electron-accepting moieties, like semiquinone-types, can react with superoxide at a high reaction rate to form quinoid structures (Samoilova et al., 2011; Zhong et al., 2019). Subsequently, the quinoid reverse to semiquinone-types by reducing Fe(III). The disproportionation of $O_2^{\bullet-}$ can be suppressed by binding on PFRs, and the PFRs facilitate electron transfer from superoxide to surface adsorbed Fe(III). Therefore, PFRs in BC facilitate the surface cycling of Fe(III)/Fe(II), and thus indirectly enhance the formation of $\bullet OH$ for pollutant decomposition. Overall, these results demonstrate the superior performance of the CaO_2/BC Fenton-like system compared to BC-lacking controls and a traditional Fenton system, as it has both a high SMX degradation rate and peroxide utilization efficiency.

4. Conclusion

Compared to traditional Fenton treatment and CaO_2-only and H_2O_2-only Fenton-like reactions without BC, the CaO_2/BC system showed enhanced removal of SMX and improved utilization efficiency of peroxides. The performance of CaO_2/BC Fenton-like reactions was correlated with the PFR content in BC. It was demonstrated that the direct interaction between BC and Fe(III) or H_2O_2 to regenerate Fe(II) is sluggish and negligible. However, PFRs serve as electron shuttles to increase the ability of superoxide radicals to regenerate Fe(II) in the CaO_2/BC system, and accordingly promote the generation of hydroxyl radicals in Fenton-like reactions (as illustrated in the graphical abstract) even at circum-neutral pH. The enhanced participation of superoxide can also mitigate the unproductive consumption of peroxides to produce molecular oxygen, as well as augment the generation of hydroxyl
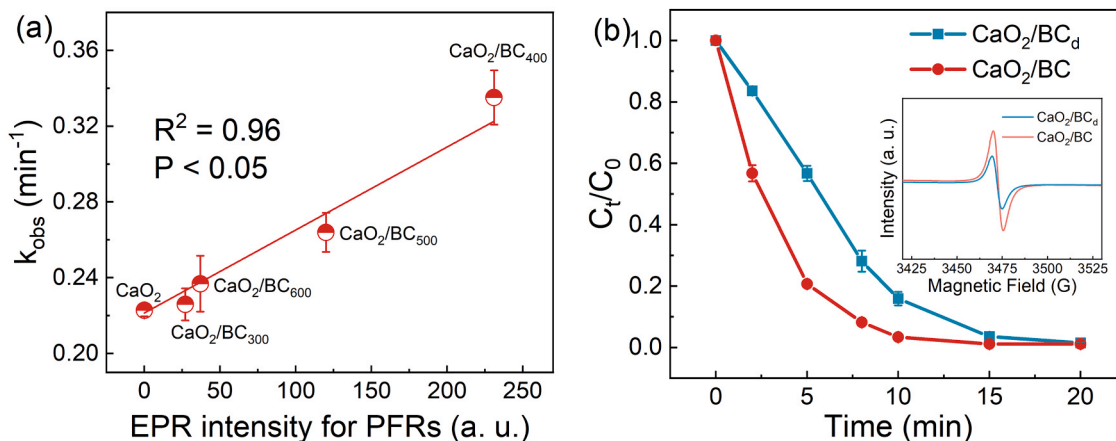
Fig. 6. Importance of persistent free radicals (PFR) in biochar. (a) Correlation between SMX degradation rate constants and the EPR signal intensity for different composites; (b) The decrease of SMX degradation by using the composite with the depleted BC, inset is the EPR spectra showing PFR signal intensity for CaO_2/BC and CaO_2/BC_d (CaO_2/BC_d is obtained from the BC with depleted PFRs, $[SMX]_0 = 10$ mg/L, $[Fe(III)] = 0.6$ mM, $n_{Fe}:n_{TA} = 1:2$, [peroxides] = 1.2 mM).

radicals. This provides a novel strategy to enhance the utilization efficiency of both peroxides and superoxide radicals by combining PFRs in BC and solid metal peroxides, and offers mechanistic insight to accelerate the rate-limiting Fe(III) reduction in Fenton-like reactions.

Although CaO_2 is not a common oxidant in Fenton-like reactions, it has great potential to mitigate logistical challenges associated with storage and transportation of the more commonly used H_2O_2. Furthermore, CaO_2-based Fenton-like reactions have superior performance over H_2O_2-based systems at circum-neutral pH. The proposed approach to enhance the participation of superoxide radicals by PFRs in biochar would enhance CaO_2-based Fenton-like reactions to efficiently remove recalcitrant organic contaminants in water treatment or soil remediation efforts.

CRediT authorship contribution statement

Shuqi Zhang: Data curation, Methodology, Investigation, Visualization, Writing – original draft. **Yan Wei**: Methodology, Investigation, Visualization. **Jordin Metz**: Visualization, Validation, Writing – review & editing. **Shengbing He**: Resources, Investigation. **Pedro J. J. Alvarez**: Resources, Validation, Writing – review & editing. **Mingce Long**: Conceptualization, Supervision, Funding acquisition, Resources, Writing – review & editing.

Declaration of Competing Interest

The authors declare that they have no known competing financial interests or personal relationships that could have appeared to influence the work reported in this paper.

Acknowledgements

Appendix A. Supplementary data

The detailed information about materials and their sources; GC/MS analysis of HCA; method for dissolved Fe(II) detection; kinetic analysis of superoxide formation rates; FTIR, XRD, SEM and XPS analysis of samples; SMX degradation, release of H_2O_2, TOC removal, open-circuit potential curves, quenching tests, EPR spectra measurements of ●OH, $O_2^{\bullet-}$ and PFRs in different systems.

Appendix A. Supporting information

Supplementary data associated with this article can be found in the online version at doi:10.1016/j.jhazmat.2021.126805.

References

Ali, M., Danish, M., Tariq, M., Ahmad, A., Shahzad Ayub, K., Lyu, S., 2020. Mechanistic insights into the degradation of trichloroethylene by controlled release nano calcium peroxide activated by iron species coupled with nano iron sulfide. Chem. Eng. J. 399, 125754.

Ali, M., Tariq, M., Sun, Y., Huang, J., Gu, X., Ullah, S., Nawaz, M.A., Zhou, Z., Shan, A., Danish, M., Lyu, S., 2021. Unveiling the catalytic ability of carbonaceous materials in Fenton-like reaction by controlled-release CaO_2 nanoparticles for trichloroethylene degradation. J. Hazard. Mater. 416, 125935.

Barreiro, J.C., Capelato, M.D., Martin-Neto, L., Bruun Hansen, H.C., 2007. Oxidative decomposition of atrazine by a Fenton-like reaction in a H_2O_2/ferrihydrite system. Water Res. 41, 55–62.

Buxton, G.V., Greenstock, C.L., Helman, W.P., Ross, A.B., 1988. Critical review of rate constants for reactions of hydrated electrons, hydrogen atoms and hydroxyl radicals (·OH/·O⁻) in aqueous solution. J. Phys. Chem. Ref. Data 17, 513–886.

Chacón, F.J., Sánchez-Monedero, M.A., Lezama, L., Cayuela, M.L., 2020. Enhancing biochar redox properties through feedstock selection, metal preloading and post-pyrolysis treatments. Chem. Eng. J. 395, 125100.

Chen, F., Ma, W., He, J., Zhao, J., 2002. Fenton degradation of malachite green catalyzed by aromatic additives. J. Phys. Chem. A 106, 9485–9490.

Chen, Y., Wang, R., Duan, X., Wang, S., Ren, N.Q., Ho, S.H., 2020. Production, properties and catalytic applications of sludge derived biochar for environmental remediation. Water Res. 187, 116390.

Dou, X., Zhang, Q., Shah, S.N.A., Khan, M., Uchiyama, K., Lin, J.M., 2019. MoS_2-quantum dot triggered reactive oxygen species generation and depletion: responsible for enhanced chemiluminescence. Chem. Sci. 10 (2), 497–500.

Duan, X., Sun, H., Shao, Z., Wang, S., 2018. Nonradical reactions in environmental remediation processes: uncertainty and challenges. Appl. Catal. B: Environ. 224, 973–982.

Fang, G., Liu, C., Gao, J., Dionysiou, D.D., Zhou, D., 2015. Manipulation of persistent free radicals in biochar to activate persulfate for contaminant degradation. Environ. Sci. Technol. 49, 5645–5653.

Furman, O., Laine, D.F., Blumenfeld, A., Teel, A.L., Shimizu, K., Cheng, I.F., Watts, R.J., 2009. Enhanced reactivity of superoxide in water–solid matrices. Environ. Sci. Technol. 43, 1528–1533.

Guo, Z., Ren, G., Jiang, C., Lu, X., Zhu, Y., Jiang, L., Dai, L., 2015. High performance heteroatoms quaternary-doped carbon catalysts derived from shewanella bacteria for oxygen reduction. Sci. Rep. 5, 17064.

Han, D., Wan, J., Ma, Y., Wang, Y., Huang, M., Chen, Y., Li, D., Guan, Z., Li, Y., 2014. Enhanced decolorization of orange G in a Fe(II)-EDDS activated persulfate process by accelerating the regeneration of ferrous iron with hydroxylamine. Chem. Eng. J. 256, 316–323.

Hayyan, M., Hashim, M.A., AlNashef, I.M., 2016. Superoxide ion: generation and chemical implications. Chem. Rev. 116, 3029–3085.

Hou, X., Huang, X., Jia, F., Ai, Z., Zhao, J., Zhang, L., 2017. Hydroxylamine promoted goethite surface Fenton degradation of organic pollutants. Environ. Sci. Technol. 51, 5118–5126.

Huang, J., Jones, A., Waite, T.D., Chen, Y., Huang, X., Rosso, K.M., Kappler, A., Mansor, M., Tratnyek, P.G., Zhang, H., 2021. Fe(II) redox chemistry in the environment. Chem. Rev. 121, 8161–8233. https://doi.org/10.1021/acs.chemrev.0c01286.

Huang, W., Brigante, M., Wu, F., Mousty, C., Hanna, K., Mailhot, G., 2013. Assessment of the Fe(III)–EDDS complex in Fenton-like processes: from the radical formation to the degradation of bisphenol A. Environ. Sci. Technol. 47, 1952–1959.

Javed, H., Metz, J., Eraslan, T.C., Mathieu, J., Wang, B., Wu, G., Tsai, A.L., Wong, M.S., Alvarez, P.J.J., 2020. Discerning the relevance of superoxide in PFOA degradation. Environ. Sci. Technol. Lett. 7, 653–658.

Klupfel, L., Keiluweit, M., Kleber, M., Sander, M., 2014. Redox properties of plant biomass-derived black carbon (biochar). Environ. Sci. Technol. 48, 5601–5611.

Li, X., Xie, Y., Jiang, F., Wang, B., Hu, Q., Tang, Y., Luo, T., Wu, T., 2020. Enhanced phosphate removal from aqueous solution using resourceable nano-CaO_2/BC composite: behaviors and mechanisms. Sci. Total Environ. 709, 136123.

Li, Y., Sun, J., Sun, S.P., 2016. Mn^{2+}-mediated homogeneous Fenton-like reaction of Fe (III)-NTA complex for efficient degradation of organic contaminants under neutral conditions. J. Hazard. Mater. 313, 193–200.

Liao, S., Pan, B., Li, H., Zhang, D., Xing, B., 2014. Detecting free radicals in biochars and determining their ability to inhibit the germination and growth of corn, wheat and rice seedlings. Environ. Sci. Technol. 48, 8581–8587.

Liu, G., Zhang, Y., Yu, H., Jin, R., Zhou, J., 2020. Acceleration of goethite-catalyzed Fenton-like oxidation of ofloxacin by biochar. J. Hazard. Mater. 397, 122783.

Liu, Y., Zhao, Y., Wang, J., 2021. Fenton/Fenton-like processes with in-situ production of hydrogen peroxide/hydroxyl radical for degradation of emerging contaminants: advances and prospects. J. Hazard. Mater. 404, 124191.

Miao, J., Geng, W., Alvarez, P.J.J., Long, M., 2020. 2D N-doped porous carbon derived from polydopamine-coated graphitic carbon nitride for efficient nonradical activation of peroxymonosulfate. Environ. Sci. Technol. 54, 8473–8481.

Mitchell, S.M., Ahmad, M., Teel, A.L., Watts, R.J., 2014. Degradation of perfluorooctanoic acid by reactive species generated through catalyzed H_2O_2 propagation reactions. Environ. Sci. Technol. Lett. 1, 117–121.

Nosaka, Y., Nosaka, A.Y., 2017. Generation and detection of reactive oxygen species in photocatalysis. Chem. Rev. 117, 11302–11336.

Pan, Y., Su, H., Zhu, Y., Vafaei Molamahmood, H., Long, M., 2018. CaO_2 based Fenton-like reaction at neutral pH: accelerated reduction of ferric species and production of superoxide radicals. Water Res. 145, 731–740.

Pham, A.L.-T., Lee, C., Doyle, F.M., Sedlak, D.L., 2009. A silica-supported iron oxide catalyst capable of activating hydrogen peroxide at neutral pH values. Environ. Sci. Technol. 43, 8930–8935.

Pignatello, J.J., Oliveros, E., MacKay, A., 2006. Advanced oxidation processes for organic contaminant destruction based on the Fenton reaction and related chemistry. Crit. Rev. Environ. Sci. Technol. 36, 1–84.

Qin, J., Cheng, Y., Sun, M., Yan, L., Shen, G., 2016. Catalytic degradation of the soil fumigant 1,3-dichloropropene in aqueous biochar slurry. Sci. Total Environ. 569–570, 1–8.

Qin, J., Zhang, S., Zhu, Y., Radian, A., Long, M., 2021. Calcium superphosphate as an inorganic stabilizer for modified-Fenton treatment of diesel-contaminated soil with two different exogenous iron sources. J. Clean. Prod. 294, 126255.

Qin, Y., Song, F., Ai, Z., Zhang, P., Zhang, L., 2015. Protocatechuic acid promoted alachlor degradation in Fe(III)/H_2O_2 Fenton system. Environ. Sci. Technol. 49, 7948–7956.

Rastogi, A., Al-Abed, S.R., Dionysiou, D.D., 2009. Effect of inorganic, synthetic and naturally occurring chelating agents on Fe(II) mediated advanced oxidation of chlorophenols. Water Res. 43, 684–694.

Rose, A.L., Waite, T.D., 2005. Reduction of organically complexed ferric iron by superoxide in a simulated natural water. Environ. Sci. Technol. 39, 2645–2650.

Samoilova, R.I., Crofts, A.R., Dikanov, S.A., 2011. Reaction of superoxide radical with quinone molecules. J. Phys. Chem. A 115, 11589–11593.

Sanchez, M., Hadasch, A., Fell, R.T., Meunier, B., 2001. Key role of the phosphate buffer in the H_2O_2 oxidation of aromatic pollutants catalyzed by Iron tetrasulfophthalocyanine. J. Catal. 202, 177–186.

Sawyer, D.T., Valentine, J.S., 1981. How super is superoxide? Acc. Chem. Res. 14, 393–400.

Smith, B.A., Teel, A.L., Watts, R.J., 2004. Identification of the reactive oxygen species responsible for carbon tetrachloride degradation in modified Fenton's systems. Environ. Sci. Technol. 38, 5465–5469.

Sun, P., Liu, H., Feng, M., Zhang, X., Fang, Y., Zhai, Z., Sharma, V.K., 2021. Dual nonradical degradation of acetaminophen by peroxymonosulfate activation with highly reusable and efficient N/S co-doped ordered mesoporous carbon. Sep. Purif. Technol. 268, 118697.

Tang, S., Wang, Z., Yuan, D., Zhang, C., Rao, Y., Wang, Z., Yin, K., 2020. Ferrous ion-tartaric acid chelation promoted calcium peroxide Fenton-like reactions for simulated organic wastewater treatment. J. Clean. Prod. 268, 122253.

Thomas, N., Dionysiou, D.D., Pillai, S.C., 2021. Heterogeneous Fenton catalysts: a review of recent advances. J. Hazard. Mater. 404, 124082.

Tian, S.Q., Wang, L., Liu, Y.L., Yang, T., Huang, Z.S., Wang, X.S., He, H.Y., Jiang, J., Ma, J., 2019. Enhanced permanganate oxidation of sulfamethoxazole and removal of dissolved organics with biochar: formation of highly oxidative manganese intermediate species and in situ activation of biochar. Environ. Sci. Technol. 53, 5282–5291.

Wang, H., Zhao, Y., Li, T., Chen, Z., Wang, Y., Qin, C., 2016. Properties of calcium peroxide for release of hydrogen peroxide and oxygen: a kinetics study. Chem. Eng. J. 303, 450–457.

Wang, J., Tang, J., 2021a. Fe-based Fenton-like catalysts for water treatment: Preparation, characterization and modification. Chemosphere 276, 130177.

Wang, J., Wang, S., 2019a. Preparation, modification and environmental application of biochar: a review. J. Clean. Prod. 227, 1002–1022.

Wang, X., Chen, N., Liu, X., Shi, Y., Ling, C., Zhang, L., 2021b. Ascorbate guided conversion of hydrogen peroxide to hydroxyl radical on goethite. Appl. Catal. B: Environ. 282, 119558.

Wang, Z., Qiu, W., Pang, S., Jiang, J., 2019b. Effect of chelators on the production and nature of the reactive intermediates formed in Fe(II) activated peroxydisulfate and hydrogen peroxide processes. Water Res. 164, 114957.

Wei, Y., Zhang, J., Zheng, Q., Miao, J., Alvarez, P., Long, M., 2021. Quantification of photocatalytically-generated hydrogen peroxide in the presence of organic electron donors: interference and reliability considerations. Chemosphere 279, 130556.

Wu, B., Su, L., Dai, X., Chai, X., 2018. Development of sludge-derived mesoporous material with loaded nano CaO_2 and doped Fe for re-utilization of dewatered waste-activated sludge as dewatering aids. Chem. Eng. J. 335, 161–168.

Wu, D., Bai, Y., Wang, W., Xia, H., Tan, F., Zhang, S., Su, B., Wang, X., Qiao, X., Wong, P. K., 2019. Highly pure MgO_2 nanoparticles as robust solid oxidant for enhanced Fenton-like degradation of organic contaminants. J. Hazard. Mater. 374, 319–328.

Xin, S., Liu, G., Ma, X., Gong, J., Ma, B., Yan, Q., Chen, Q., Ma, D., Zhang, G., Gao, M., Xin, Y., 2021. High efficiency heterogeneous Fenton-like catalyst biochar modified $CuFeO_2$ for the degradation of tetracycline: economical synthesis, catalytic performance and mechanism. Appl. Catal. B: Environ. 280, 119386.

Xing, M., Xu, W., Dong, C., Bai, Y., Zeng, J., Zhou, Y., Zhang, J., Yin, Y., 2018. Metal sulfides as excellent co-catalysts for H_2O_2 decomposition in advanced oxidation processes. Chem 4, 1–14.

Xu, Z., Xu, X., Zhang, Y., Yu, Y., Cao, X., 2020. Pyrolysis-temperature depended electron donating and mediating mechanisms of biochar for Cr(VI) reduction. J. Hazard. Mater. 388, 121794.

Xue, Y., Sui, Q., Brusseau, M.L., Zhou, W., Qiu, Z., Lyu, S., 2019. Insight into CaO_2-based Fenton and Fenton-like systems: strategy for CaO_2-based oxidation of organic contaminants. Chem. Eng. J. 361, 919–928.

Yan, Q., Lian, C., Huang, K., Liang, L., Yu, H., Yin, P., Zhang, J., Xing, M., 2021. Constructing an acidic microenvironment by MoS_2 in heterogeneous Fenton reaction for pollutant control. Angew. Chem. Int. Ed. 60, 17155–17163.

Yan, S., Kim, M., Salley, S.O., Ng, K.Y.S., 2009. Oil transesterification over calcium oxides modified with lanthanum. Appl. Catal. A: Gen. 360, 163–170.

Yang, D., Qu, D., An, L., Zong, X., Sun, Z., 2021. A metal-free carbon dots for wastewater treatment by visible light active photo-Fenton-like reaction in the broad pH range. Chin. Chem. Lett. 32, 2292–2296.

Yang, J., Pan, B., Li, H., Liao, S., Zhang, D., Wu, M., Xing, B., 2016. Degradation of p-nitrophenol on biochars: role of persistent free radicals. Environ. Sci. Technol. 50, 694–700.

Yang, Z., Yu, A., Shan, C., Gao, G., Pan, B., 2018. Enhanced Fe(III)-mediated Fenton oxidation of atrazine in the presence of functionalized multi-walled carbon nanotubes. Water Res. 137, 37–46.

Yang, Z., Qian, J., Yu, A., Pan, B., 2019. Singlet oxygen mediated iron-based Fenton-like catalysis under nanoconfinement. Proc. Natl. Acad. Sci. U.S.A. 116, 6659–6664.

Yi, Q., Ji, J., Shen, B., Dong, C., Liu, J., Zhang, J., Xing, M., 2019. Singlet oxygen triggered by superoxide radicals in a molybdenum cocatalytic Fenton reaction with enhanced REDOX activity in the environment. Environ. Sci. Technol. 53, 9725–9733.

Yu, L., Yuan, Y., Tang, J., Wang, Y., Zhou, S., 2015. Biochar as an electron shuttle for reductive dechlorination of pentachlorophenol by geobacter sulfurreducens. Sci. Rep. 5, 16221.

Yuan, D., Zhang, C., Tang, S., Li, X., Tang, J., Rao, Y., Wang, Z., Zhang, Q., 2019. Enhancing CaO_2 Fenton-like process by Fe(II)-oxalic acid complexation for organic wastewater treatment. Water Res. 163, 114861.

Żeglinski, J., Piotrowski, G.P., Piękos, R., 2006. A study of interaction between hydrogen peroxide and silica gel by FTIR spectroscopy and quantum chemistry. J. Mol. Struct. 794, 83–91.

Zhang, Y., Xu, X., Cao, L., Ok, Y.S., Cao, X., 2018. Characterization and quantification of electron donating capacity and its structure dependence in biochar derived from three waste biomasses. Chemosphere 211, 1073–1081.

Zhao, N., Yin, Z., Liu, F., Zhang, M., Lv, Y., Hao, Z., Pan, G., Zhang, J., 2018. Environmentally persistent free radicals mediated removal of Cr(VI) from highly saline water by corn straw biochars. Bioresour. Technol. 260, 294–301.

Zhong, D., Zhang, Y., Wang, L., Chen, J., Jiang, Y., Tsang, D.C.W., Zhao, Z., Ren, S., Liu, Z., Crittenden, J.C., 2018. Mechanistic insights into adsorption and reduction of hexavalent chromium from water using magnetic biochar composite: key roles of Fe_3O_4 and persistent free radicals. Environ. Pollut. 243, 1302–1309.

Zhong, D., Jiang, Y., Zhao, Z., Wang, L., Chen, J., Ren, S., Liu, Z., Zhang, Y., Tsang, D.C. W., Crittenden, J.C., 2019. pH dependence of arsenic oxidation by rice-husk-derived biochar: roles of redox-active moieties. Environ. Sci. Technol. 53, 9034–9044.

Zhou, P., Ren, W., Nie, G., Li, X., Duan, X., Zhang, Y., Wang, S., 2020. Fast and long-lasting iron(III) reduction by boron toward green and accelerated Fenton chemistry. Angew. Chem. Int. Ed. 59, 16517–16526.

Zhu, L., Ji, J., Liu, J., Mine, S., Matsuoka, M., Zhang, J., Xing, M., 2020a. Designing 3D-MoS_2 sponge as excellent cocatalysts in advanced oxidation processes for pollutant control. Angew. Chem. Int. Ed. 59, 13968–13976.

Zhu, Y., Qin, J., Zhang, S., Radian, A., Long, M., 2020b. Solid peroxides in Fenton-like reactions at near neutral pHs: superior performance of MgO_2 on the accelerated reduction of ferric species. Chemosphere 270, 128639.